A Study of the Frictional Layer of TiAl-12Ag-5TiB$_2$ Composite During Dry Sliding Wear

Zengshi Xu, Jie Yao, Xiaoliang Shi, Wenzheng Zhai, Ahmed Mohamed Mahmoud Ibrahim, Yecheng Xiao, Long Chen, Qingshuai Zhu, and Ao Zhang

Many studies have shown that the excellent tribological properties of materials are primarily attributed to the formation of expected frictional layer on the worn surface. This article is dedicated to explore the possible formation and acting mechanism of frictional layer of TiAl-12Ag-5TiB$_2$ composite. At normal load of 12 N, a frictional layer that consists of wear-induced layer and plastic deformation layer is observed. The soft wear-induced layer supported by the harder plastic deformation layer leads to the low friction coefficient and high wear resistance. The harder plastic deformation layer is induced by repetitive tribo-contact and considerable plastic deformation. Its high hardness improves the wear resistance of composite, and fine-grained structure promotes the diffusion of lubricating phase during dry friction process. The soft wear-induced layer can be divided into tribofilm and mechanically mixed layer. The mechanically mixed layer that consists of Ag and Ti-Al Oxides can continuously be provided to the worn surface to form a tribofilm with low shearing stress junctions, lowering the friction coefficient.

1. Introduction

Along with the rapid development of modern industrial manufacturing and scientific technology, some moving mechanical parts are requested to work under extreme operational conditions, i.e., aerospace, high speeds and loads, very low or high temperatures, and high vacuum conditions where liquid lubricants fail to work. These parts have to withstand wear, and provide low friction to promote energy efficiency. Concerning these scenarios, the most traditional metals cannot suffice the industrial needs due to the inadequacies of mechanical and tribological properties. Consequently, metal matrix self-lubricating composites (MMSCs) are good alternative, attaining better advantages in many cases such as lighter weight, longer durability, higher reliability, and less loss (Ref 1, 2). As the race for better materials performance is never ending, attempts to develop viable MMSCs for better tribological performance continue.

According to the definition of self-lubricating ceramic composites in Ref 3, the concept of MMSCs can be described that the specific functions of various types of additives are added to metal matrix materials to improve their tribological behavior. MMSCs which possess a low friction coefficient combined with high mechanical strength and wear resistance have a better adaptability under extreme application conditions. High mechanical and tribological performance is a result of the combination of both the characteristics of metal matrix materials and tribological properties of additives. As a kind of high-performance structural materials as well as functional materials with a great application potential in special conditions, MMSCs that consist of different metallic matrix and different additives have been extensively investigated by many engineers and researchers in the field of tribology in recent decades (Ref 4-7). Since people noticed that the use of solid lubricants could effectively enhance the antifriction and wear resistance of metallic matrix, compounds (MoS$_2$, WS$_2$, h-BN), low-melting metals (Ag, Sn, Pb), inorganic fluorides (LiF$_2$, CaF$_2$, BaF$_2$), and some oxides (ZnO, CuO, MoO$_3$) had been successfully employed as solid lubricants (Ref 8, 9). Moreover, it is widely reported that intensifying with hard phases is a good alternative to improving the hardness and wear resistance of a softer substrate without significantly changing other properties, such as density. Improvement in wear resistance by incorporating hard ceramic particles like TiB$_2$, Al$_2$O$_3$, B$_4$C, and SiC into the based alloys is well known (Ref 10).

Numerous studies have been conducted on the friction and wear properties of MMSCs. Most of them have revealed that thin layers, so-called tribofilms, are observed on the wear surfaces. The tribofilm can be formed on the contact surface under the action of large plastic strains during dry sliding process, is beneficial for the purpose of antifriction and wear resistance properties (Ref 7). Alexeyev et al. (Ref 11) used a slip-line field analysis to analyze the process of deformation and flow of a soft phase toward the sliding interface for self-lubricating metal matrix composites. Their results showed that properties of both matrix and soft second phase as well as shape and size of second phase controlled the formation of tribofilm. Bushe et al. (Ref 12) built a model to analyze the tribofilm thickness for aluminum-alloy composition. The model explained that the soft phase exuded to the surface of the alloy from a subsurface layer in which the plastic flow of the soft phase occurred. The extrusion of the soft phase was caused by the matrix deformation which could be both elastic and plastic in this subsurface layer.

Zengshi Xu, Jie Yao, Xiaoliang Shi, Wenzheng Zhai, Ahmed Mohamed Mahmoud Ibrahim, Yecheng Xiao, Long Chen, Qingshuai Zhu and **Ao Zhang**, School of Mechanical and Electronic Engineering, Wuhan University of Technology, 122 Luoshi Road, Wuhan 430070, China. Contact e-mail: sxl071932@126.com.

It is well known that sliding contact between ductile materials often induces large plastic strains in the near-surface regions, and the corresponding subsurface structure will be changed accordingly due to local deformation (Ref 13). Lieblich et al. (Ref 14) presented qualitative and quantitative results for the subsurface modifications that occurred as a consequence of sliding wear. They found three regions beneath a worn surface: (1) a layer that usually contained a mixture of the sliding materials and the counterface material and oxides, known as the tribolayer or the mechanically mixed layer, beneath which was followed by (2) a plastically deformed region, and (3) the non-affected region. Friction characterized by plastic deformation results in formation of a frictional layer with gradient structure that consists of a sequence of layers with different deformation. The tribofilm mentioned above is the upmost plastically deformed layer of frictional layer. It is well recognized that the beneficial effect of self-lubricating composite depends on the thickness of the frictional layer, the relative mechanical properties of the frictional layer and substrate as well as the contact pressure carried by the frictional layer and substrate (Ref 15). The frictional layer of self-lubricating composite has a remarkable effect on its tribological properties. Understanding of the structural features and formation mechanism of frictional layer during sliding contact is crucial for the development of tribology and lubrication failure of materials.

As a potential new structural material used as aerospace and automotive parts for turbine blades, bearings, and exhaust valves, TiAl matrix self-lubricating composites attract extensive attention due to their low density, high strength-to-weight ratio, self-lubricity, and wearability. However, few studies have been conducted to study the formation mechanism and structural features of the frictional layer which plays an important role on the wear behaviors. In this study, TiAl as metal matrix, Ag as solid lubricant, and TiB_2 as reinforced phase are used to fabricate TiAl matrix self-lubricating composite. The TiAl-12Ag-5TiB_2 (wt.%) composite is prepared by in situ technique using spark plasma sintering (SPS) which can lead to a better improvement in mechanical properties and tribological properties (Ref 16). Dry sliding friction and wear experiments of TiAl-12Ag-5TiB_2 composite under several applied loads are carried out on a ball-on-disk high-temperature tribometer to obtain frictional layers. Accordingly, the chief aim of the present study is to investigate the structural features, formation, and acting mechanism of frictional layers with applied loads. These results provide a clue for the optimization design of TiAl composite materials related to the self-lubricating function.

2. Materials and Methods

2.1 Materials and Processing

TiAl-12Ag-5TiB_2 was prepared by SPS using a D.R.Sinter® SPS3.20 (Sumitomo Coal & Mining, now SPS Syntex Inc.)

apparatus at 1100 °C under a pressure of 35 MPa for 10 min in pure Ar atmosphere protection. TiAl had poor ductility at ambient temperatures and low creep resistance at elevated temperatures, which largely limited their applications. Alloying was a promising method to overcome these inherent deficiencies of TiAl, e.g., Nb, Si, V, Mn, and Cr. Ti-46Al-2Cr-2Nb alloys showed both improved ductility at ambient temperatures and creep resistance at elevated temperatures compared to the single-phase TiAl (Ref 17). Therefore, Ti-46Al-2Cr-2Nb alloys were chosen as the substrate material in the work. The composite powders of TiAl matrix consisted of Ti, Al, Nb, and Cr powders with molar ratio of 50:46:2:2. Commercially available Ti, Al, Nb, Cr, Ag, and TiB_2 were used as the starting powders. The information about the starting powders is listed in Table 1. The mass fractions of Ag and TiB_2 were 12 and 5 wt.%, respectively. Before SPS, the starting powders were mixed by high-energy ball-milling in vacuum for 10 h and were dried in a vacuum drying oven at room temperature (RT) for 10 h. The as-prepared sample surfaces were ground to remove the layers on the surfaces and polished mechanically with emery papers down to 1200 grit, 5 μm up to a mirror finish, to make the following tests. The measured density was determined by Archimedes' principle according to the ASTM: B962-13 (Ref 18). Ten tests were conducted, and the mean value (4.17 ± 0.02 g/cm^3) was given.

2.2 Tribological Experiments

The dry sliding friction and wear experiments were performed on a HT-1000 ball-on-disk high-temperature tribometer (made in Zhong Ke Kai Hua Corporation, China) for 60 min at the temperature of RT (about 25 °C), a sliding speed of 0.2 m/s, and a relative humidity of about 65% according to the ASTM: G99-05 (Ref 19). The contact schematic sketch of the ball-on-disk pair is shown in Fig. 1. The disk, which was the as-prepared sample, rotated with a constant speed. The counterface was a Si_3N_4 ceramic ball with a diameter of 6 mm, holding under the normal load. Dry sliding tests were conducted at different normal loads of 2, 7, 12, and 22 N, respectively. A new commercial Si_3N_4 ceramic ball (15 GPa,
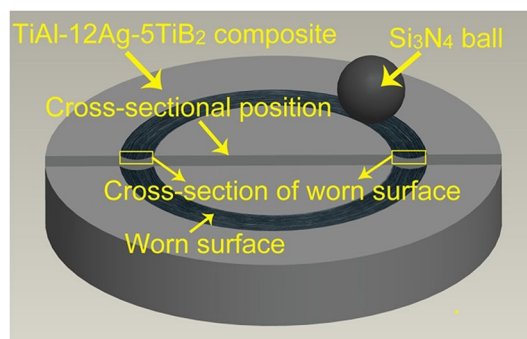
Fig. 1 The contact schematic sketch of the ball-on-disk pair and cross section for preparing FESEM and nanoindentation

Table 1 The information about the starting powders

Starting powders	Ti	Al	Nb	Cr	Ag	TiB_2
Average size (μm)	20	20	10	10	25	4
Purity (%)	99.9	99.9	99.9	99.9	99.9	99.9

Ra 0.01 µm) was chosen before each test. The friction coefficients were automatically measured and recorded in real time by the computer system of the friction tester. The cross-section profile of worn surface was measured using a surface profilometer. The wear volume V was determined $V = AL$, where A was the cross-section area of worn scar, and L was the perimeter of the worn scar. The wear rate was calculated by the following formula $W = V/SF_N$, where V was the wear volume, S was the sliding distance, and F_N was the normal load (Ref 20). This was calculated as a function of the wear volume divided by the sliding distance S and the applied load N, and expressed as mm^3/N m. The tests for every given conditions were repeated three times to obtain reliable data. The average value was used as the evaluating data.

2.3 Microstructure Analysis

The surface of the as-prepared sample was examined by XRD with Cu Kα radiation at 30 kV and 40 mA at a scanning speed of $0.01 \ s^{-1}$ for the identification of the phase constitution. Microstructure and surface composition of the as-prepared sample before frictional test were analyzed using electron probe microanalysis (EPMA, JAX-8230) and energy dispersive spectroscopy (EDS, GENESIS 7000). The morphologies and compositions of worn surfaces of sample obtained at several normal loads were also analyzed using EPMA, EDS, and x-ray photoelectron spectroscope (XPS) for the investigation of wear mechanisms. For investigating the microstructure of frictional layer, mechanical cutting was performed using an IsoMet®1000 precision cutting machine perpendicular to the sliding direction of the worn surface of TiAl-12Ag-5TiB₂ composite after friction test at load of 12 N as shown in Fig. 1. The microstructure of fracture cross section of worn surface was observed by a field emission scanning electron microscope (FESEM, FEI-SIRION). Then, the cross section was carefully polished with emery papers down to 2000 grit, and handled by vibration polishing with an alumina suspension (Buehler VibroMet® 2 Vibratory Polisher). The morphology of polished cross section of worn surface was analyzed by FESEM. The hardness and elastic modulus were calculated from the load and depth data obtained by nanoindentation on the frictional layer and TiAl matrix at different indentation loads of 3000, 50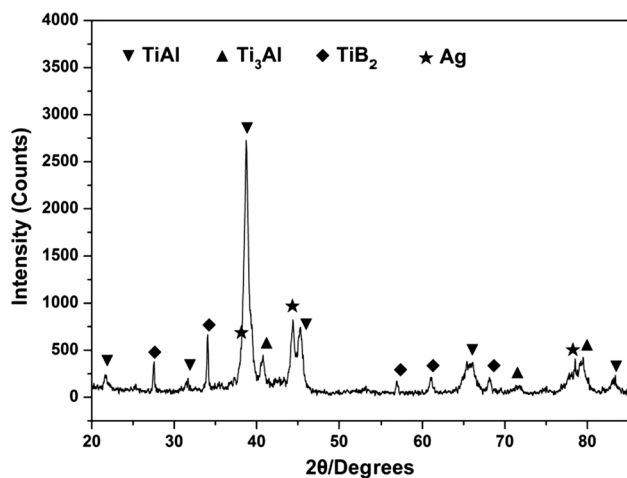00, 7000, and 9000 µN using a nanomechanical test instrument (HYSITRON, INC.). Loading and unloading steps were performed on the TiAl-12Ag-5TiB₂ composite to examine the deformation, making sure that the valid data used for analysis purposes were mostly elastic.

3. Results

3.1 Compositions

Figure 2 shows the XRD pattern of the as-prepared sample. The pattern shows the peaks corresponding to the presence of TiAl, Ag, and TiB₂. Figure 3 shows the microstructure of the as-prepared sample. The elemental composition of different regions marked A, B, and C has been given in Table 2. It implies that the gray area is the continuous bulk TiAl phase, and the dark gray area is the TiB₂ phase, while the light gray area is the Ag phase. It is also clear that the TiB₂ phase has a scattered distribution which is surrounded by the continuous bulk TiAl phase and the scattered Ag phase. It indicates that the lubricating phase Ag and the reinforced phase TiB₂ have a uniform distribution in TiAl-12Ag-5TiB₂ composite.

3.2 Friction and Wear Behavior

Figure 4(a) shows the variation of the apparent friction coefficients with applied loads at a sliding speed of 0.2 m/s. The friction coefficient is found to decrease as the load increases from 2 to 12 N, and then increase after beyond this load. The inserted Fig. 4(b) presents the typical friction coefficient curves at different loads. One could observe relatively larger fluctuations in the friction response at 2 N, in comparison to other larger loads. When the load is over 2 N, the friction coefficient undergoes acute fluctuation at the initial stage, and then stabilizes around a constant value with the sliding duration. Fluctuating time of the friction coefficient seems to be shorter at higher applied loads, suggesting that steady-state wear is easier to approach at high load. The behavior of the friction coefficient with an evident fluctuation at the initial stage followed by a stabilization period in a low value is attributed to the formation of frictional layer on the interface of TiAl-12Ag-5TiB₂ composite (Ref 21). The wear rate of sample as a function of the normal load for tests is plotted in Fig. 5. From Fig. 5, it can be observed that
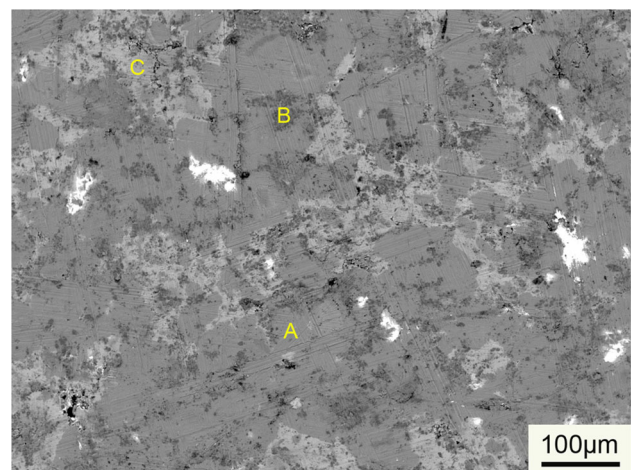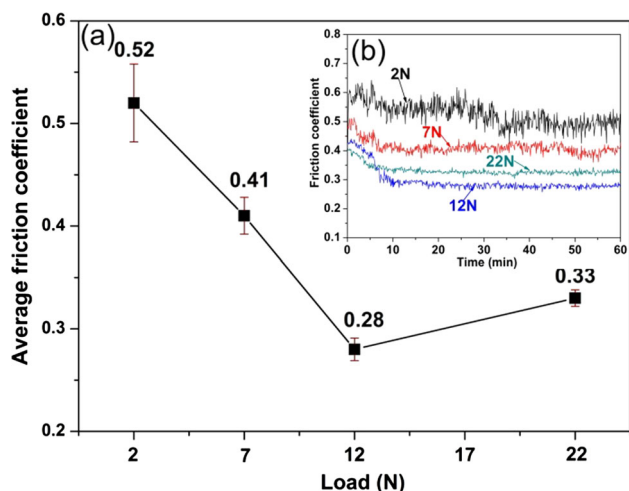

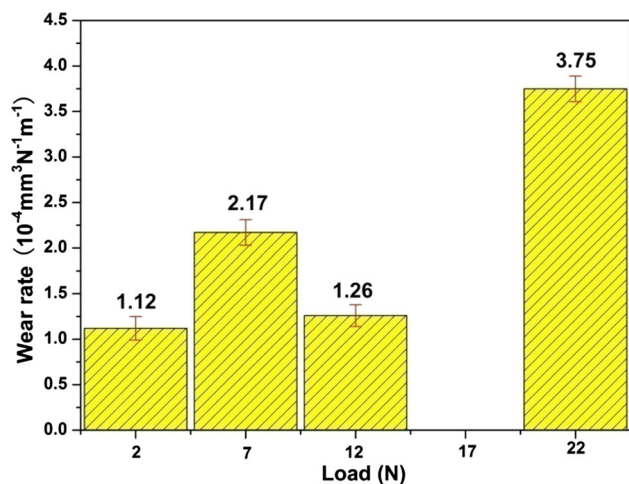**Fig. 2** XRD pattern of TiAl-12Ag-5TiB₂ composite

Fig. 3 Microstructure of TiAl-12Ag-5TiB₂ composite

Table 2 EDS analysis of element (wt.%) in different regions of microstructure

Region	Element, wt.%					
	Ti	Al	Nb	Cr	Ag	B
A (gray)	57.19	39.13	1.67	2.01	…	…
B (dark gray)	65.02	4.24	…	…	1.03	29.71
C (light gray)	7.89	5.74	…	…	86.37	…

Fig. 4 (a) Variation of the apparent friction coefficients with applied loads. (b) The typical friction coefficient curves at different loads

Fig. 5 Variations of wear rates of TiAl-12Ag-5TiB$_2$ composite with applied loads

the wear rate firstly increases and then decreases with the increase of load at the range of 2-12 N. But when the load increases to up to 22 N, the wear rate steeply increases by about 3 times compared to that at 12 N.
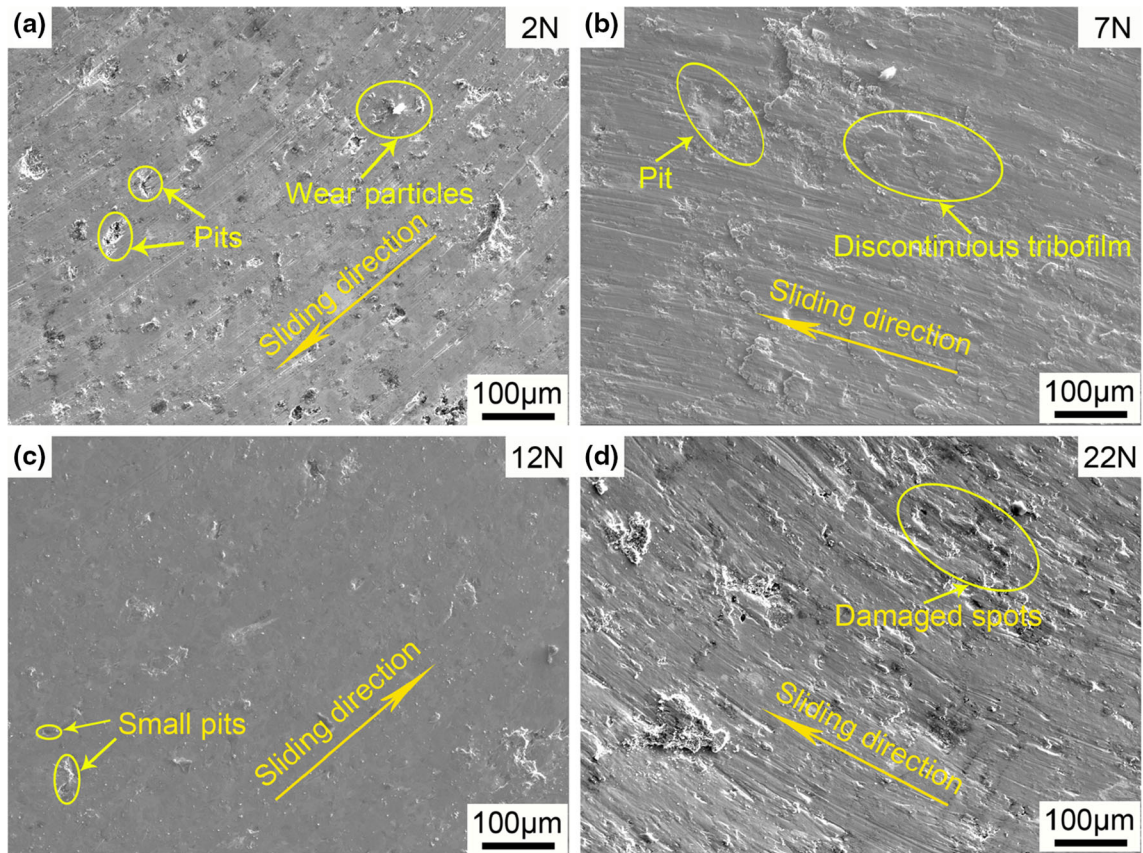
3.3 Worn Surfaces and Cross-Sections

Figure 6 exhibits the typical EPMA morphologies of worn surfaces of TiAl-12Ag-5TiB$_2$ composite tested at various loads (Ref 16). It is observed that the severity of plastic deformation is increasing with the increase in load. The different morphologies of the worn surfaces clearly indicate that the wear mechanism

changes with the increment of load. Under the load of 2 N, the main wear mechanism is characterized by abrasive wear. It is evident from some fine scratches, wear particles, and abrupt pits visible on the worn surface in the sliding direction. The possible reason is that the hard surface protuberance of Si$_3$N$_4$ ball generates the impact load that induces an ultra high instantaneous contact stress, resulting in irreversible destruction on the worn surface. With the increase in applied load, frictional layers are formed on the worn surfaces. Under the load of 7 N, some discrete flake debris adheres tightly to the worn surface and forms a discontinuous island-like tribofilm. Meanwhile, scratches and pits are also found on the worn surface. The morphology of worn surface reveals that a mix abrasive-adhesive wear mechanism dominates the wear process. Under the load of 12 N, no scratches can be found on the worn surface which shows a flat surface covered by a continuous tribofilm with small pits. The morphology of worn surface undoubtedly suggests that the main wear mechanism is adhesive wear. As the applied load increases up to 22 N, the locally damaged and even fractured spots are observed on the deformed worn surface. Under high load, the protective film can no longer remain stable under the plowing action and serious deformation.

According to the above results, it can be summed up as follows: the formation of tribofilm is associated with applied load. Under lower loads (less than 2 N), the fine scratches and abrupt pits are formed on the worn surface by abrasive wear, the tribofilm cannot be formed; under higher loads (high than 22 N), the tribofilm cannot remain stable and cover the worn surface under the plowing action and serious deformation; as the load increases from 7 to 12 N, the worn surface is gradually covered by continuous smooth tribofilm. Since the tribofilm is well formed at the load of 12 N, the sample exhibits the best tribological behavior with the friction coefficient of 0.28 and the wear rate of 1.26×10^{-4} mm^3/N m.

In order to investigate the formation mechanism and structure evolution of frictional layer, the typical FESEM micrographs underneath the worn surface of TiAl-12Ag-5TiB$_2$ composite at applied load of 12 N are presented in Fig. 7 and 8 (Ref 16). The microstructural observation position is shown in Fig. 1. Figure 7 shows the FESEM micrographs of polished cross section of worn surface. As shown in Fig. 7(a), a wear-induced layer is formed due to the circular sliding of Si$_3$N$_4$ counterface ball on the same wear track of TiAl-12Ag-5TiB$_2$ composite. Figure 7(b) shows a high magnification micrograph of area A marked by a dotted yellow rectangle in Fig. 7(a), where the wear-induced layer can be more clearly observed. The significant stratification morphology is easily identified, and the wear-induced layer consists of two distinct layers remarked as B and C in Fig. 7(b). The layer B is a tribofilm which often forms on the worn surface of MMSC with the friction process (Ref 16). Tribofilm may play an important role in the sliding wear behaviors of composites. The layer C is mechanically mixed layer which contains abundant Ag and O

Fig. 6 The typical EPMA morphologies of worn surfaces of TiAl-12Ag-5TiB$_2$ composite tested at various loads
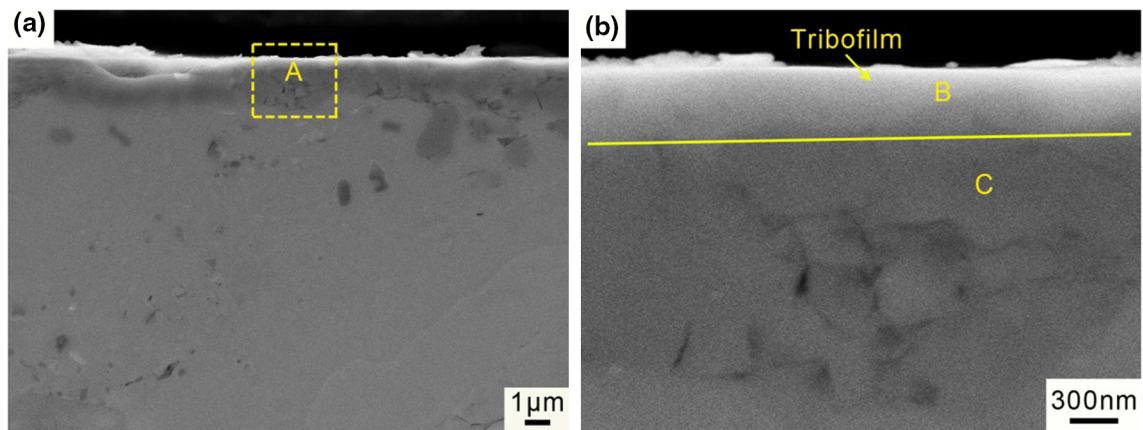
Fig. 7 (a) The FESEM micrograph of polished cross section of worn surface at load of 12 N; (b) A high magnification micrograph of area A marked by a dotted yellow rectangle in Fig.7a

elements as suggested by the EDS analysis. It indicates that Ag diffuses to the sliding surface, and oxides are generated during cyclic sliding friction process under the applied contact pressure. To further confirm the oxide formation, the XPS analysis is used herein. It can be found from Fig. 8 that the peaks assigned to TiO$_2$ and Al$_2$O$_3$ are detected, proving the formation of Ti-Al Oxides. The higher temperature is necessary to the formation of oxides. Therefore, we now estimate the temperature of the worn surface caused by the accumulation of frictional heat. We made our attempt to calculate frictional heat using the methods suggested by Kannel and Barber (Ref 22),

which were particularly applicable to a pin-on-disk geometry and time-averages of the heat transfer over individual cycles (Ref 23). The local surface temperature on the sliding surface where the frictional heat occurs during sliding contact can be written as Ref 23:
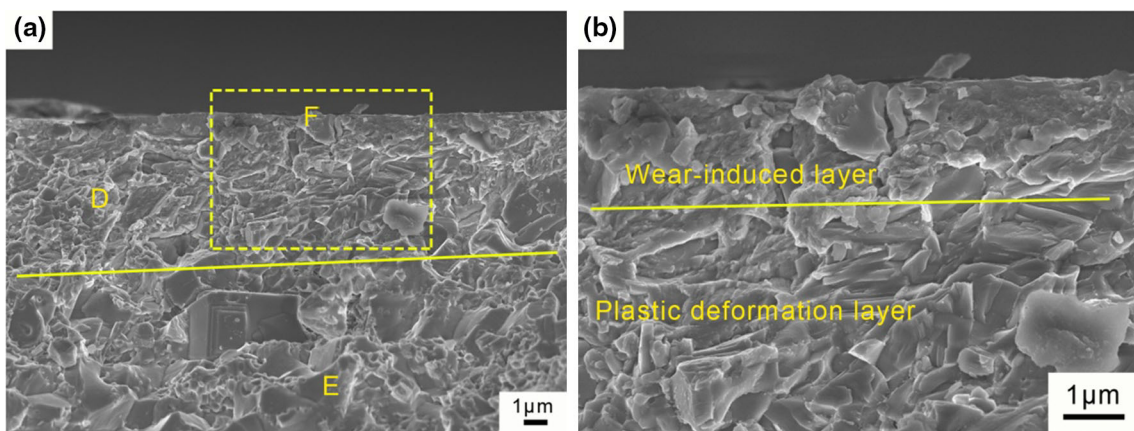
$$T = \frac{Q_A}{h_s}\left\{1 - \mathrm{erfc}\left[h_s\sqrt{\frac{t}{K\rho c}}\right]\exp\left[\frac{h_s^2 t}{K\rho c}\right]\right\}, \qquad \text{(Eq 1)}$$

where h_s is the heat transfer coefficient for convection ($\sim$20 W/m^2 K in air), t is the time, and K, ρ, and c are the
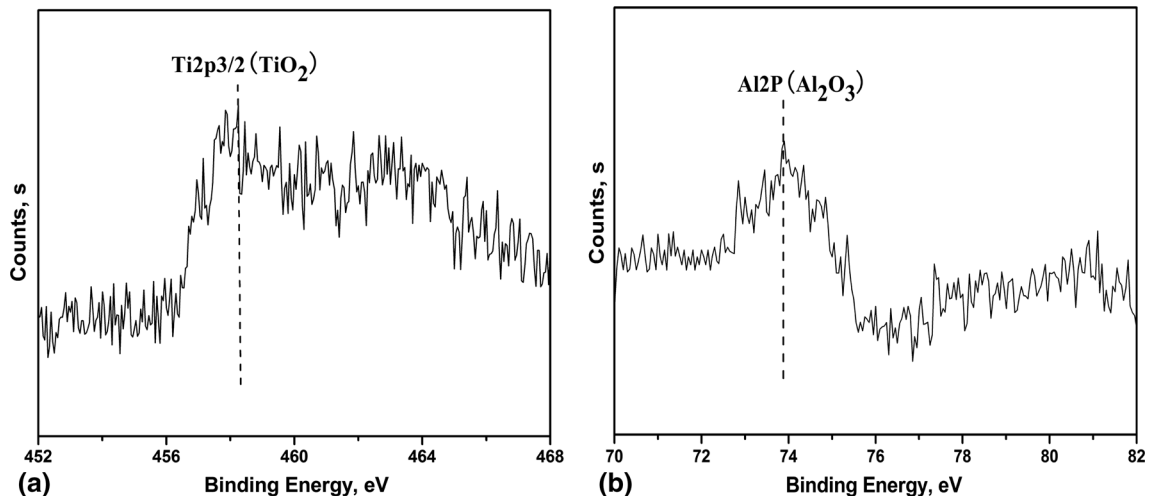
Fig. 8 XPS spectra of elements on worn surface of TiAl-12Ag-5TiB$_2$ composite at applied load of 12 N: (a) Ti, (b) Al

Fig. 9 (a) The FESEM micrograph of fractured cross section of worn surface at load of 12 N; (b) A high magnification micrograph of area F marked by a dotted yellow rectangle in (a)

thermal conductivity, density, and specific heat, respectively, of the substrate material. Q_A is the frictional heat power per unit area and is given by

$$Q_A = \frac{\mu P \nu}{A_s}, \qquad \text{(Eq 2)}$$

where μ is the friction coefficient, P is the normal load, ν is the sliding velocity, and A_S is the surface area of the wear track. For the TiAl-12Ag-5TiB$_2$ composite, the thermal conductivity ($\sim$15 W/m K) and specific heat ($\sim$0.6 J/g K) of TiAl given by Ref 24 are used, while the density and friction coefficient are obtained from experimental measurements. Hence, we calculate the local surface temperature in our experiments using Eq 1 as 515 °C. Even if this value is assumed to hold over the entire duration of a 1 h experiment, and the test temperature will be below 400 °C in the most stages of friction test, it is certainly enough for the oxidation reaction. Figure 9 shows the FESEM micrographs of fracture cross section of worn surface. As shown in Fig. 9(a), the microstructure evolution underneath the worn surface is evident and different stratification can be found below the wear-induced layer. It may be due to that the subsurface undergoes different levels of plastic strain along the depth from the worn surface. The regions with different morphologies are marked as layer D and E. Layer D is plastic deformation layer, and layer E is non-affected layer (TiAl matrix). It can be found that the grain in layer D is finer than that in layer E. Figure 9(b) shows a high magnification micrograph of area F marked by a dotted yellow rectangle in Fig. 9(a), where the grain structure of plastic deformation layer can be more clearly observed. As shown in Fig. 9(b), the grains are refined or elongated below the wear-induced layer to suppress further shear deformation during sliding process.

The above results reveal a series of microstructure evolution in the subsurface regions of worn surface at the contact load of 12 N, and the wear properties follow expectations based on the microstructure. As the hardness affects the friction wear properties, a study of the relationship between hardness and microstructure under the worn surface is conducted using a nanomechanical test instrument. Since the depth-sensitive nanoindentation has the capability to characterize mechanical properties at micrometer scales, the variations of hardness and elastic modulus in wear-induced layer, plastic deformation layer, and TiAl matrix are calculated from the load and depth

data obtained by multiple nanoindentation measurements at different indentation load levels. Figure 10 shows the surface profile of cross section of worn surface with residual indentations in three layers. Figure 11 shows the typical nanoindentation load-depth profiles of three layers at indentation loads of 3000 and 9000 µN. It is evident that extensive plastic deformation can take place underneath the indenter without detectable cracking and phase transitions. It may be contributed to the inelastic displacements (Ref 25). In load-depth profiles, lower indentation depths indicate higher hardness, and higher slopes of unloading curves indicate high stiffness or elastic modulus of the samples (Ref 26). As shown in Fig. 11(a), at the load of 3000 µN, the indentation depths in wear-induced layer, plastic deformation layer and matrix are 132, 93, and 104 nm, respectively. As shown in Fig. 11(b), at the load of 9000 µN, the indentation depths in wear-induced layer, plastic deformation layer, and matrix are 240, 173, and 189 nm, respectively. The indentation of plastic deformation layer shows the shallowest depth, suggesting that plastic deformed structure exhibits higher hardness. However, the total penetration depth into the wear-induced layer is the deepest, indicating that the hardness of the wear-induced layer is lower than that of the plastic deformation layer.
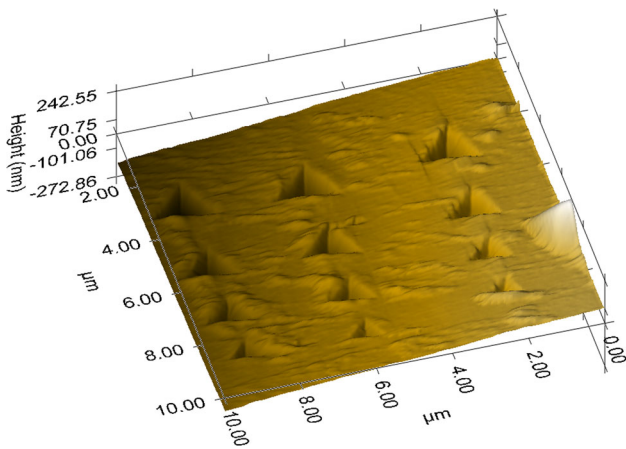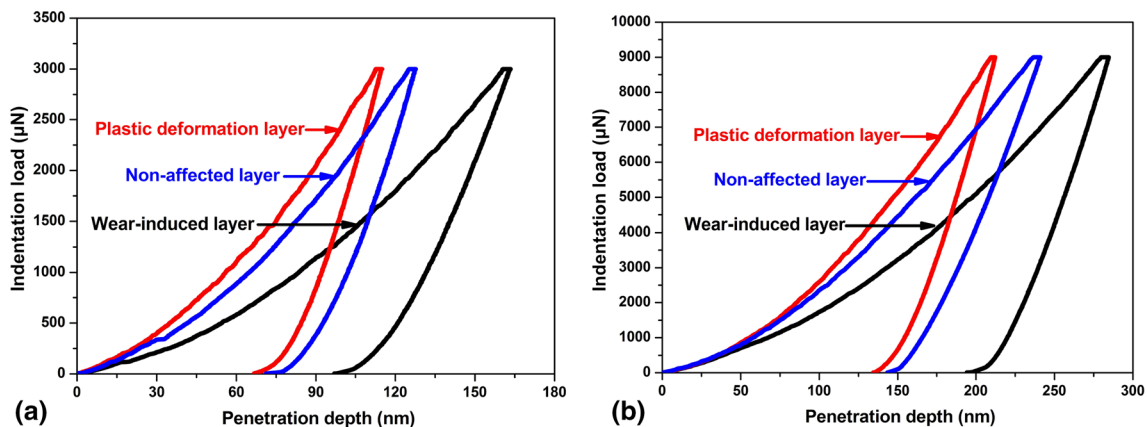
The hardness and elastic modulus for different layers at different indentation load levels are plotted in Fig. 12, indicating that the hardness and elastic modulus are slightly dependent on the indentation loads. The average hardness and elastic modulus values for each layer are listed in Table 3. The wear-induced layer has lower hardness (30.9%) and elastic modulus (15.7%) than the matrix. The plastic deformation layer has higher hardness (28.4%) and elastic modulus (36.6%) than the matrix. Such comparison confirms the above-measured depths of indentation for the different layers.

4. Discussion

4.1 The Formation Mechanism of Frictional Layer

Friction and wear behaviors of TiAl-12Ag-5TiB$_2$ composite at different normal loads are tested. Friction at 2 N is accompanied by relatively higher value of the friction coefficient and larger fluctuation in the friction response, in comparison to other larger loads. Neither obvious plastically deformed region nor tribofilm is visible on the worn surface, and some fine scratches, wear particles, and abrupt pits are found instead. The reason may be that the low applied load such as 2 N cannot generate enough plastic strain in the near-surface region, and then no well structural change can appear. The sample shows a low friction coefficient of 0.28 and a low wear rate of 1.26×10^{-4} mm^3/N m at the applied load of 12 N due to the formation of a great frictional layer. As the applied load increases up to 22 N, the friction coefficient keeps a low value of 0.33, but the wear rate steeply increases by about 3 times which is 3.75×10^{-4} mm^3/N m. The obvious plastically deformed region fractured spots are observed on the worn surface. It shows that the large applied load such as 22 N will produce large shear stress which is higher than interfacial bond strength, and the shear stress causes breakdown and fracture of worn surface that results in the removal of materials. Jungk et al. (Ref 27) studied the role of substrate plasticity on the tribological behavior of diamond-like nanocomposite coatings and explained the similar phenomenon.

As shown in Fig. 7 and 8, the multi-layered structure is presented during dry sliding process at applied load of 12 N. The top layer is a wear-induced layer, beneath which is followed by a plastically deformation layer and a non-affected

Fig. 10 The surface profile of cross section of worn surface with residual indentations in three layers

Fig. 11 The typical nanoindentation load-depth profiles of three layers at indentation loads of 3000 (a) and 9000 µN (b)

layer. The complete frictional layer consisting of the wear-induced layer and the plastically deformation layer possesses superior antifriction effect on the friction surface and plays the role in protecting the worn surface. The cross section of worn surface at 12 N exhibited exactly the changes in microstructure expected, with distinct wear-induced layer and plastically deformation layer which occur for different formation process. Hence, we make our attempt to investigate the evolution of the microstructure on the wear-induced layer and plastically deformation layer to further research the formation of the frictional layer during the sliding process.

As mentioned previously, the wear-induced layer consists of tribofilm and mechanically mixed layer which are in the topmost frictional layer. The thickness of the tribofilm is in the range of 200-300 nm, and the thickness of the mechanically mixed layer is in the range of 1.2-2 μm, depending on the location of the measurement in Fig. 7(b). The main composition of the mechanically mixed layer is Ag and a mixture of Ti-Al Oxides as suggested by the XPS analysis. It indicates that the formation of the mechanically mixed layer is related to the diffusion of lubricating phase and the oxidation of the matrix materials. Deng et al. (Ref 3) explained that the soft second phase in the ceramic matrix was squeezed out and smeared on the contact surface under the normal and friction force during the sliding tests. The soft materials were transferred from the pores and cracks in the matrix to the surface, and it was found that the experimental conditions such as load, sliding velocity, and temperature had an important effect on the transfer of soft phase (Ref 28). The oxidation of the matrix materials is resulted from frictional heat generated on the worn surface due to friction.

The microstructural morphologies in the plastically deformation layer are obviously different from those in the matrices, which are induced by repetitive tribo-contact and considerable
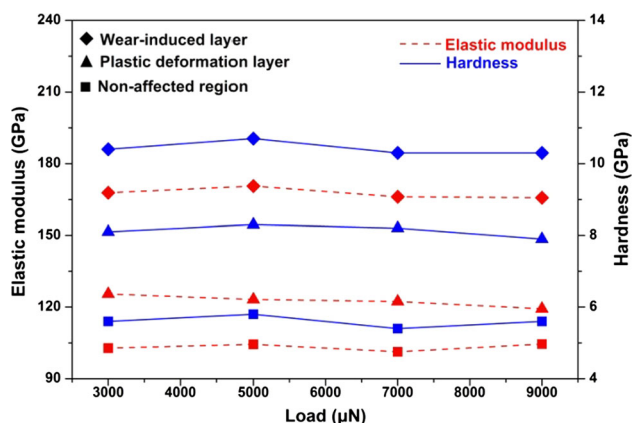
plastic deformation. During dry friction process, the worn surface undergoes cyclic extrusion stress and severe shear stress which induce large plastic strain in the near-surface region. Material initially near the surface is heated and deformed by the cyclic extrusion stress and severe shear stress. Since the worn surface of materials is severely deformed by wear, both the temperature and strain increase simultaneously as results of frictional heat and local deformation. The grains will experience orientations along the sliding direction and unstable within the imposed additional strain field. With increase of accumulative plastic strain, the grains will be fined in order to lower the energy. Hammerberg et al. (Ref 29) anticipated that the formed ultrafined structure was commonly the results of plastic flow of material in the surface layer stressed by friction shear. This shear deformation significantly increased the equivalent strain and promoted grain refinement. As a result, the grain refinement in the worn surface layer of steel with high hardness tended to be initiated by a higher nominal shear strain and effective shear strain. It can be concluded that the effective shear strain for the plastic deformation layer promotes the refinement and stretch of the grains.

As shown in Fig. 12, the hardness and elastic modulus show slightly dependence on the indentation loads and little fluctuate with increasing load. Conversely, Guo et al. (Ref 25) demonstrated that the hardness and Young's modulus of aluminum oxynitride showed strong dependence on the applied load and obviously decreased with increasing load, particularly in the force ranging from 0 to 200 mN due to the size effect of the nanoindenter and the intrinsic plasticity. The different phenomena may be attributed to the small change of indentation load (3000-9000 μN) in this paper, which is insufficient to cause a significant influence on hardness and elastic modulus. Meanwhile, the average hardness and elastic modulus values for each layer listed in Table 3 confirm that a soft layer is produced and supported by a fine-grained harder layer. Very similar behavior has been observed in the previous study (Ref 30). Experiments with a hard bearing steel ball sliding in vacuum on various Pb-Sn and babbitt alloys indicated smooth sliding with low friction and wear (Ref 30). Cross section exhibited exactly the changes in microstructure expected, with coarsening and softening near the surface. Rigney (Ref 30) concluded that these materials created the proper conditions for low friction—a soft surface layer supported by a harder base material. Such a material system was self-repairing, with continuing deformation localized near the surface, so sliding should remain smooth.

4.2 The Acting Mechanism of the Frictional Layer

The expected frictional layer formed at normal load of 12 N plays an important role in the sliding wear behaviors of TiAl-12Ag-5TiB$_2$ composite. The analysis above demonstrates that the frictional layer consists of tribofilm, mechanically mixed layer, and plastic deformation layer. During wear process, the plastic deformation layer plays the role of wear-resistant skeleton, withstanding the plastic deformation. The nanoindentation tests for the formed frictional layer show that the plastic deformation layer possesses higher hardness (28.4%) and elastic modulus (36.6%) than the matrix. The improvement of hardness and elastic modulus will strengthen the deforming resistance of material, contributing to the improvement of wear resistance of TiAl-12Ag-5TiB$_2$ composite. Kumar et al. (Ref 31) described that the plowing tendency of the abrasive particle reduced, as the hardness of the composite increased.

Fig. 12 The hardness and elastic modulus for different layers at different indentation load levels

Table 3 The average hardness and elastic modulus values for each layer

Different region	Elastic modulus, GPa	Hardness, GPa
Wear-induced layer	103.3 ± 1.3	5.8 ± 0.2
Plastic deformation layer	167.6 ± 1.9	10.4 ± 0.2
Non-affected region	122.6 ± 2.2	8.7 ± 0.2

Moreover, the grain refinement in plastic deformation layer promotes the diffusion of lubricating phase during dry friction process. Arzt (Ref 32) explained that reduction of the grain size increased the volume fraction of the grain boundaries which acted as a path for the squeezing-out process. The nanoindentation tests for the formed frictional layer show that the mechanically mixed layer possesses lower hardness (30.9%) and elastic modulus (15.7%) than the matrix. The above analysis implies that the main composition of the mechanically mixed layer is Ag and a mixture of Ti-Al Oxides. It is well known that Ag and Ti-Al Oxides are excellent lubricants, which can form a tribofilm with low shearing stress junctions, lowering the friction coefficient (Ref 33). The friction coefficient between two smooth bodies sliding under elasticity loaded conditions in a ball-on-disk contact can be expressed as Ref 27:

$$\mu = \frac{S_0}{P} + \alpha, \qquad (Eq\ 3)$$

where μ is the friction coefficient, S_0 is interfacial shear strength, P is the mean Hertzian contact pressure of the contact, and α represents the lowest attainable friction coefficient of the friction couple. The given equation shows that the friction coefficient varies linearly with interfacial shear strength. When there is a tribofilm on the wear surface, the matrix endures the load, and friction occurs on the lubricant film. As the lubricant film on the wear surface has a much lower interfacial shear strength than the matrix and thus results in a reduced friction coefficient according to Eq 3.

According to the above analysis, the plastic deformation layer plays the role of wear-resistant skeleton, withstanding the plastic deformation, and the mechanically mixed layer that consists of Ag and Ti-Al Oxides can be continuously provided to the worn surface to form a tribofilm with low shearing stress junctions. The expected frictional layer formed at normal load of 12 N plays an important role in the sliding wear behaviors of TiAl-12Ag-5TiB$_2$ composite. It is found that the composite possesses superior antifriction and wear resistance during wear process at normal load of 12 N.

5. Conclusions

The dry friction and wear behaviors of TiAl-12Ag-5TiB$_2$ composite under varying normal loads are systematically researched through the determination of friction coefficients and wear rates. The composite exhibits the excellent tribological properties with the friction coefficient of 0.28 and the wear rate of 1.26×10^{-4} mm^3/N m at normal load of 12 N due to the formation of expected frictional layer. The formation and acting mechanism are discussed according to the analysis of the morphologies and compositions of cross section of worn surface. The main conclusions can be drawn as follows:

(1) The self-lubrication of TiAl-12Ag-5TiB$_2$ composite is traced to the formation of a frictional layer at the worn surface, and the formation of frictional layer is controlled by the applied loads.

(2) The frictional layer consists of wear-induced layer and plastic deformation layer. The wear-induced layer has lower hardness (30.9%) and elastic modulus (15.7%) than the matrix, whereas the plastic deformation layer has higher hardness (28.4%) and elastic modulus (36.6%)

than the matrix. The specific microstructure with a soft layer produced and supported by a harder layer leads to the low friction coefficient and high wear resistance.

(3) The wear-induced layer which is in the topmost frictional layer consists of tribofilm and mechanically mixed layer. The main composition of the mechanically mixed layer is Ag and a mixture of Ti-Al Oxides. The formation of the mechanically mixed layer is related to the diffusion of lubricating phase and the oxidation of the matrix materials.

(4) The plastic deformation layer exhibits a different microstructure with refined or elongated grains. Since the worn surface of materials is severely deformed by wear, both the temperature and strain increase simultaneously as results of frictional heat and local deformation. The grains will experience orientations along the sliding direction and unstable within the imposed additional strain field. With increase of accumulative plastic strain, the grains will be fine in order to lower the energy.

(5) The plastic deformation layer plays the role of wear-resistant skeleton, withstanding the plastic deformation due to its higher hardness. Moreover, the grain refinement in plastic deformation layer promotes the diffusion of lubricating phase during dry friction process. The soft mechanically mixed layer that consists of Ag and Ti-Al Oxides can be continuously provided to the worn surface to form a tribofilm with low shearing stress junctions, lowering the friction coefficient.

References

1. J.P. Giltrow, Series-Composite Materials and the Designer: Article 4: Friction and Wear of Self-Lubricating Composite Materials, *Composites*, 1973, **4**, p 55–64

2. M.N. Gardos, Self-Lubricating Composites for Extreme Environment Applications, *Tribol. Int.*, 1982, **15**, p 273–283

3. J.X. Deng and T.K. Cao, Self-Lubricating Mechanisms via the In Situ Formed Tribofilm of Sintered Ceramics with CaF$_2$ Additions When Sliding Against Hardened Steel, *Int. J. Refract. Met. Hard Mater.*, 2007, **25**, p 189–197

4. Z.S. Xu, X.L. Shi, W.Z. Zhai, J. Yao, S.Y. Song, and Q.X. Zhang, Preparation and Tribological Properties of TiAl Matrix Composites Reinforced by Multilayer Graphene, *Carbon*, 2014, **67**, p 168–177

5. X.L. Shi, S.Y. Song, W.Z. Zhai, M. Wang, Z.S. Xu, J. Yao, Q.D. Abid, and Q.X. Zhang, Tribological Behavior of Ni3Al Matrix Self-Lubricating Composites Containing WS$_2$, Ag and hBN Tested from Room Temperature to 800 °C, *Mater. Des.*, 2014, **55**, p 75–84

6. S.Y. Zhu, Q.L. Bi, M.Y. Niu, J. Yang, and W.M. Liu, Tribological Behavior of NiAl Matrix Composites with Addition of Oxides at High Temperatures, *Wear*, 2012, **274**, p 423–434

7. D.S. Xiong, Lubrication Behavior of Ni-Cr-based Alloys Containing MoS$_2$ at High Temperature, *Wear*, 2001, **251**, p 1094–1099

8. R. Tyagi, D.S. Xiong, J.L. Li, and J.H. Dai, Elevated Temperature Tribological Behavior of Ni Based Composites Containing Nano-silver and hBN, *Wear*, 2010, **269**, p 886–890

9. G. Hammes, R. Schroeder, C. Binder, A.N. Klein, and J.D.B. Mello, Effect of Double Pressing/Double Sintering on the Sliding Wear of Self-Lubricating Sintered Composites, *Tribol. Int.*, 2014, **70**, p 119–127

10. K.L. Tee, L. Lu, and M.O. Lai, Wear Performance of In-Situ Al-TiB$_2$ Composite, *Wear*, 2000, **240**, p 59–64

11. N. Alexeyev and S. Jahanmir, Mechanics of Friction in Self-Lubricating Composite Materials I: Mechanics of Second-Phase Deformation and Motion, *Wear*, 1993, **166**, p 41–48

12. N.A. Bushe, I.G. Goryacheva, and Y.Y. Makahovskaya, Effects of Aluminum-Alloy Composition on Self-Lubrication of the Frictional Surfaces, *Wear*, 2003, **254**, p 1276–1280

13. B. Yao, Z. Han, Y.S. Li, N.R. Tao, and K. Lu, Dry Sliding Tribological Properties of Nanostructured Copper Subjected to Dynamic Plastic Deformation, *Wear*, 2011, **271**, p 1609–1616

14. M. Lieblich, J. Corrochano, J. Ibáñez, V. Vadillo, J.C. Walker, and W.M. Rainforth, Subsurface Modifications in Powder Metallurgy Aluminium Alloy Composites Reinforced with Intermetallic MoSi$_2$ Particles Under Dry Sliding Wear, *Wear*, 2014, **309**, p 126–133

15. M. Valefi, M. Rooij, M. Mokhtari, and D.J. Schipper, Modelling of a Thin Soft Layer on a Self-Lubricating Ceramic Composite, *Wear*, 2013, **303**, p 178–184

16. J. Yao, X.L. Shi, W.Z. Zhai, A.M.M. Ibrahim, Z.S. Xu, S.Y. Song, L. Chen, Q.S. Zhu, Y.C. Xiao, and Q.X. Zhang, Effect of TiB$_2$ on Tribological Properties of TiAl Self-Lubricating Composites Containing Ag at Elevated Temperature, *J. Mater. Eng. Perform.*, 2015, **24**, p 307–318

17. J. Cheng, J. Yang, X.H. Zhang, H. Zhong, J.Q. Ma, F. Li, L.C. Fu, Q.L. Bi, J.S. Li, and W.M. Liu, High Temperature Tribological Behavior of a Ti-46Al-2Cr-2Nb Intermetallics, *Intermetallics*, 2012, **31**, p 120–126

18. American Society for Testing and Materials. Standard test methods for density of compacted or sintered powder metallurgy (PM) products using Archimedes' principle, ASTM B962-13; 2013

19. American Society for Testing and Materials, Standard test method for wear testing with a pin-on-disk apparatus, ASTM G99-05; 2005

20. A. Kolubaev, S. Tarasov, O. Sizova, and E. Kolubaev, Scale-Dependent Subsurface Deformation of Metallic Materials in Sliding, *Tribol. Int.*, 2010, **43**, p 695–699

21. S.Y. Zhu, Q.L. Bi, J. Yang, and W.M. Liu, Tribological Property of Ni$_3$Al Matrix Composites with Addition of BaMoO$_4$, *Tribol. Lett.*, 2011, **43**, p 55–63

22. J.W. Kannel and S.A. Barber, Estimate of Surface Temperature During Rolling Contact, *Tribol. Trans.*, 1989, **32**, p 305–310

23. T.J. Rupert and C.A. Schuh, Sliding Wear of Nanocrystalline Ni-W: Structural Evolution and The Apparent Breakdown of Archard Scaling, *Acta Mater.*, 2010, **58**, p 4137–4148

24. W.J. Zhang, B.V. Reddy, and S.C. Deevi, Physical Properties of TiAl-Base Alloys, *Scripta Mater.*, 2001, **45**, p 645–651

25. J.J. Guo, K. Wang, T. Fujita, J.W. McCauley, J.P. Singh, and M.W. Chen, Nanoindentation Characterization of Deformation and Failure of Aluminum Oxynitride, *Acta Mater.*, 2011, **59**, p 1671–1679

26. B. Bhushan, B.K. Gupta, and M.H. Azarian, Nanoindentation, Microscratch, Friction and Wear Studies of Coatings for Contact Recording Applications, *Wear*, 1995, **181**, p 743–758

27. J.M. Jungk, J.R. Michael, and S.V. Prasad, The Role of Substrate Plasticity on the Tribological Behavior of Diamond-Like Nanocomposite Coatings, *Acta Mater.*, 2008, **56**, p 1956–1966

28. K. Sang, Z. Lü, and Z. Jin, A Study of the SiC-L Composite Ceramics for Self-Lubrication, *Wear*, 2002, **253**, p 1188–1193

29. J.E. Hammerberg, B.L. Holian, J. Roeder, A.R. Bishop, and S.J. Zhou, Nonlinear Dynamics and the Problem of Slip at Material Interfaces, *Phys. D: Nonlinear Phenom.*, 1998, **123**, p 330–340

30. D.A. Rigney, Comments on the Sliding Wear of Metals, *Tribol. Int.*, 1997, **30**, p 361–367

31. S. Kumar, V. Subramanya Sarma, and B.S. Murty, Influence of In Situ Formed TiB$_2$ Particles on the Abrasive Wear Behaviour of Al-4Cu Alloy, *Mater. Sci. Eng.*, 2007, **465**, p 160–164

32. E. Arzt, Size Effects in Materials Due to Microstructural and Dimensional Constraints: A Comparative Review, *Acta Mater.*, 1998, **46**, p 5611–5626

33. X.L. Shi, J. Yao, Z.S. Xu, W.Z. Zhai, S.Y. Song, M. Wang, and Q.X. Zhang, Tribological Performance of TiAl Matrix Self-Lubricating Composites Containing Ag, Ti$_3$SiC$_2$ and BaF$_2$/CaF$_2$ Tested from Room Temperature to 600 °C, *Mater. Des.*, 2014, **53**, p 620–633